

Exploring of point-contact spectra of $\text{Ba}_{1-x}\text{Na}_x\text{Fe}_2\text{As}_2$ in the normal and superconducting state

Yu. G. Naidyuk, O. E. Kvitnitskaya

*B. Verkin Institute for Low Temperature Physics and Engineering,
National Academy of Sciences of Ukraine, 47 Lenin Ave., 61103, Kharkiv, Ukraine*

S. Aswartham, G. Fuchs, K. Nenkov, S. Wurmehl

Leibniz-Institut für Festkörper- und Werkstoffforschung Dresden e.V., Postfach 270116, D-01171 Dresden, Germany

We present study of derivatives of current-voltage $I(V)$ characteristics of point-contacts (PCs) based on $\text{Ba}_{1-x}\text{Na}_x\text{Fe}_2\text{As}_2$ ($x=0.25$) in the normal and superconducting state. The detailed analysis of $dV/dI(V)$ data (also given in Appendix A) shows that the thermal regime, when temperature increases with a voltage at a rate of about 1.8 K/mV, is realized in the investigated PCs at least at high biases V above the superconducting (SC) gap Δ . In this case, specific resistivity $\rho(T)$ in PC core is responsible for a peculiar $dV/dI(V)$ behavior, while a pronounced asymmetry of $dV/dI(V)$ is caused by large value of thermopower in this material. A reproducible zero-bias minima detected on $dV/dI(V)$ at low biases in the range $\pm(6-9)$ mV well below the SC critical temperature T_c could be connected with the manifestation of the SC gap Δ . Evaluation of these Andreev-reflection-like structures on $dV/dI(V)$ points out to the preferred value of $2\Delta/k_B T_c \approx 6$. The expected second gap features on $dV/dI(V)$ are hard to resolve unambiguously, likely due to impurity scattering, spatial inhomogeneity and transition to the mentioned thermal regime as the bias further increases. Suggestions are made how to separate spectroscopic features in $dV/dI(V)$ from those caused by the thermal regime.

PACS numbers: 73.40.Jn, 74.70.Dd, 74.45.+c

I. INTRODUCTION

Yanson's point-contact (PC) spectroscopy is the time-proved technique to investigate electron-phonon (quasiparticle) interactions in solids^{1,2}. PC spectroscopy was successfully applied to a large number of simple metals and more complex conducting systems, thus it became a world-wide recognized method in the solid state physics³. One of the related (sister) branches of PC spectroscopy to investigate the superconducting (SC) state is PC Andreev-reflection (PCAR) spectroscopy. The latter is the well-reputed tool to get SC parameters from the PC differential resistance/conductance. Combining these two approaches gives the possibility to receive simultaneously information about the normal as well as the SC state properties of the matter under study. During the last years PCAR spectroscopy is widely used to investigate SC state in newly discovered iron-based superconductors (see, e.g., Ref.⁴). The most attention here is paid to the study of the SC gap(s) and its temperature and directional dependence. However, study of the normal state behavior of these materials by Yanson's PC spectroscopy attracted less attention. One of the reasons is that Yanson's PC spectroscopy of quasiparticle excitations is carried out at energies usually an order of amplitude larger than the SC gap energy. In this case shortening of the inelastic mean free path of electrons can result to violation of spectroscopy because of transition to the thermal regime when the temperature rises in the PC core by increasing a bias voltage⁵. Nevertheless, study of the normal state of iron-based superconductors by Yanson's PCs can provide helpful information as to

the current regime in PCs as well as to the quasiparticle excitations. In this paper we have carried out comprehensive PC measurements in the normal and in the SC state on single crystals of $\text{Ba}_{1-x}\text{Na}_x\text{Fe}_2\text{As}_2$ - typical member of the mentioned iron family with [122] structure.

II. EXPERIMENTAL DETAILS

Single crystals of $\text{Ba}_{1-x}\text{Na}_x\text{Fe}_2\text{As}_2$ were grown using a self-flux high temperature solution growth technique. Substitution of Ba by Na leads to the suppression of spin-density wave ordering and induces superconductivity up to 34 K at optimal doping for $x \approx 0.4$ ⁶. We studied samples with the intermediate sodium concentration $x \approx 0.25$. For a single crystals with $x \approx 0.25$ the resistivity shows a kink at $T = 117$ K (see Ref.⁶ and inset in Fig. 9), typically found in hole-doped [122]-type compounds (see, e.g., Ref.⁷). This kink is an indication of the structural and magnetic transition. Thus, the sample with $x \approx 0.25$ shows both an antiferromagnetic and a SC transition what is typically present in the underdoped [122]-type compounds. The SC transition occurs here at about 10 K⁶.

We have chosen $\text{Ba}_{1-x}\text{Na}_x\text{Fe}_2\text{As}_2$ single crystals with $x \approx 0.25$ and relative low $T_c \approx 10$ K to search for electron-quasiparticle interaction features in the normal state, that is above T_c , by Yanson's PC spectroscopy. In this case thermal resolution (smearing) of PC spectra^{2,3} of about $5.44k_B T \geq 5$ meV is still not high to prevent spectroscopic investigation. On the other hand, measuring above T_c would prevent appearance of SC features, which

isostructural system $\text{Ba}_{1-x}\text{K}_x\text{Fe}_2\text{As}_2$ ⁸.

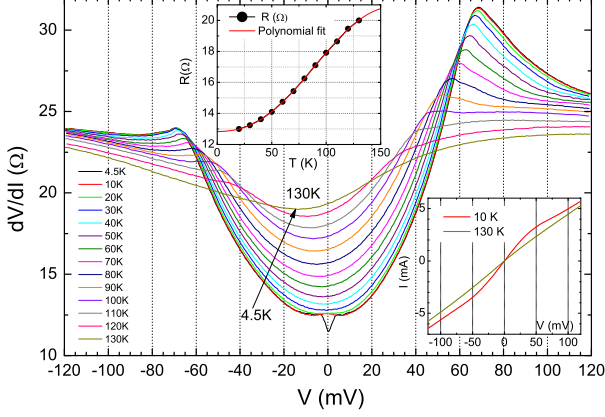


FIG. 1: (Color online) $dV/dI(V)$ measured for the $\text{Ba}_{0.75}\text{Na}_{0.25}\text{Fe}_2\text{As}_2$ -Cu PC with $R \approx 13 \Omega$ at various temperatures. Upper inset: Temperature dependence of resistance $R(T) = dV/dI(V=0, T)$ of this PC (dots) measured at $V=0$ along with a polynomial approximation (solid curve). Bottom inset: examples of $I(V)$ characteristics for PC from the main panel measured above T_c at 10 K and 130 K.

can mask quasiparticle excitations (especially in the low energy region) or may be erroneously taken as the latter. We should mention that the investigated single crystals were nonhomogeneous (at least at the surface), probably, due to volatility of Na component and showed a significant variation of the local T_c of PC as it will be shown below.

The PCs were established *in situ* by touching a sharpened Ag or Cu thin wire ($\phi \approx 0.2$ – 0.3 mm) to the cleaved (at room temperature) surface or to an edge of the sample. Thus, we have measured heterocontacts between normal metal and the title compound. The differential resistance $dV/dI(V) \equiv R(V)$ and $dV^2/dI^2(V)$ of $I(V)$ characteristic of PC were recorded by sweeping the *dc* current I on which a small *ac* current i was superimposed using the standard lock-in technique. The measurements were performed in the temperature range from 3 K up to 130 K in some cases.

III. RESULTS AND DISCUSSION

Spectroscopic information including the determination of the SC energy gap can be derived from PC measurements only if the investigated PCs are in the ballistic or in the diffusive regime of the current flow³, where electrons can gain an excess energy up to eV and heating effects are negligible. Thus, the contact size d should be smaller than the inelastic electron mean free path. To shrink a variation of the SC gap on the scale of the PC size, the PC diameter d should also be less than the SC coherence length ξ , which amounts to only 2 nm in the

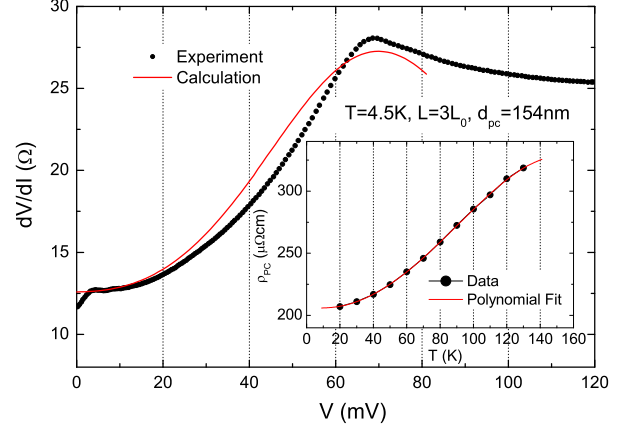


FIG. 2: (Color online) Symmetrised $dV/dI(V)$ of the PC (points) from Fig. 1 measured at $T=4.5$ K along with a calculated $dV/dI(V)$ according to Eqs. (2),(3) (solid line) with $d=154$ nm. To fit the position of the maxima we used an enhanced Lorenz number $L = 3L_0$ in the calculation. Inset: $\rho_{PC}(T)$ used for the calculations, which mimics the $R(T)$ behavior from Fig. 1 (see inset).

The PC diameter d can be estimated from its resistance R_{PC} according to Wexler's formula³:

$$R_{PC} \approx 16\rho l / 3\pi d^2 + \rho / 2d. \quad (1)$$

Here we neglect the contribution to the second term related to the resistivity of a clean normal metal (needle) and suppose geometrically equal parts occupied by each metal in our case of heterocontact. Utilizing the Drude free electron model, we estimated $\rho l \approx 1.3 \cdot 10^4 n^{-2/3} \approx 3.8 \cdot 10^{-11} \Omega \cdot \text{cm}^2$ using the electron density $n \approx 6.2 \cdot 10^{21} \text{ cm}^{-3}$ obtained from the Hall coefficient $R_H \approx 4 \cdot 10^{-3} \text{ cm}^3/\text{C}$ for $\text{Ba}_{1-x}\text{K}_x\text{Fe}_2\text{As}_2$ with $x=0.4$ ⁶. The elastic electronic mean-free path in $\text{Ba}_{0.75}\text{Na}_{0.25}\text{Fe}_2\text{As}_2$ is estimated to be about $l = \rho l / \rho_0 \sim 10$ nm using the residual resistivity of the investigated samples $\rho_0 \approx 40 \mu\Omega \text{ cm}^6$. From Eq. (1), the PC diameter d is estimated to be between 14 and 60 nm using typical PC resistance between 5 and 50 Ω . Thus, the necessary condition of the smallness of the PC size d compared to l and ξ is not fulfilled for the investigated PCs. Therefore, a distribution of SC gap is expected in the PC region and the current flow is at least diffusive. The diffusive regime itself does not prevent to get spectral information, however it favors the transition to the thermal regime with a bias rise. So, the observation of characteristic AR features in the $dV/dI(V)$ curves in the SC state is important to prove the spectral regime. Another criteria of realization of the spectral regime in PCs is the observation of phonon (quasiparticle) structures in $d^2 V/dI^2(V)$ curves in the normal state.

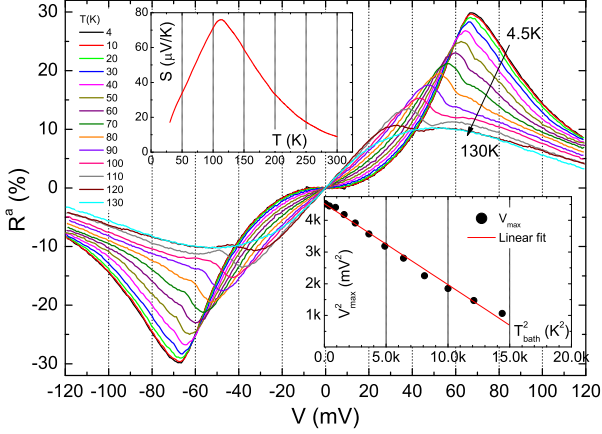


FIG. 3: (Color online) Calculated antisymmetric part $R^a(\%) = 100(R(V > 0) - R(V < 0))/2R(V = 0)$ of PC from Fig. 1 at different temperatures, here $R = dV/dI$. Right inset: Position of the maximum of R^a vs temperature in quadratic coordinates. Left inset: Temperature dependence of the thermopower S of $\text{Ba}_{0.7}\text{K}_{0.3}\text{Fe}_2\text{As}_2$ ¹⁰.

We have measured hundreds of $dV/dI(V)$ dependences of $\text{Ba}_{0.75}\text{Na}_{0.25}\text{Fe}_2\text{As}_2$ – Cu(or Ag) PCs. In general, the $dV/dI(V)$ spectra do not show any principal difference while being measured by attaching the needle to the cleaved surface or to an edge of the samples. In both cases the shape of $dV/dI(V)$ varies from one PC to another PC. This is because PC is created by chance and its microscopic structure is caused by influence of stress, surface defects, oxides, impurities etc. Therefore, we analyzed $dV/dI(V)$ to establish reproducible features in the PC spectra reflecting bulk properties.

Taking into account the short characteristic electronic lengths in the iron-based superconductors, as estimated above, and the steep resistivity rise with temperature⁶, one should distinguish carefully the spectroscopic features from those caused by thermal effects.

Characteristic $dV/dI(V)$ curves measured in a wide voltage and temperature range are shown in Fig. 1. Here, conspicuous maxima at about ± 70 mV and pronounced $dV/dI(V)$ asymmetry are seen. The maxima become broader and their position shifts to lower energies as the temperature rises. Besides, the $dV/dI(V)$ at 4.5 K displays a small zero-bias minimum, which is of SC origin because it vanishes at about 10 K, what coincides with the T_c of the bulk sample for $x = 0.25$. With temperature increase, the intensity of the main parabolic-like minimum reduces and the side maxima move to lower voltages as the temperature increases. In the inset, the temperature dependence of the PC resistance $R(T)$ (defined as $R = dV/dI(V = 0)$) is shown. Differentiating of formula (1) with respect to temperature, we find $d = (d\rho/dT)/2(dR/dT)$ and, thus, the PC size can be deter-

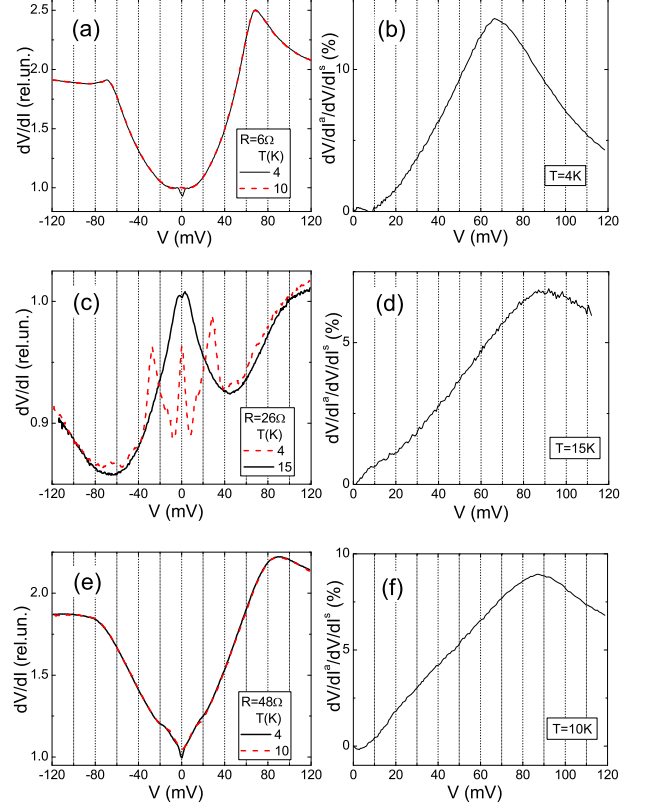


FIG. 4: (Color online) Left panels: dV/dI curves for several $\text{Ba}_{0.75}\text{Na}_{0.25}\text{Fe}_2\text{As}_2$ –Cu contacts for a broad bias range measured below and above T_c . Right panels: reduced antisymmetric part $dV/dI^a(V)/dV/dI^s(V)$ for the corresponding curves from the left panel. Here $dV/dI^s(V) = (dV/dI(V > 0) + dV/dI(V < 0))/2R(V = 0)$ is symmetric part of $dV/dI(V)$.

mined by measuring the temperature dependence of its resistance. Taking the mentioned derivatives for several temperatures between 20 and 80 K, an average diameter of about 80 nm is obtained. Using this procedure to determine the PC diameter, the real resistivity in the PC core can be derived. The residual resistivity of the PC turned out to be about $\rho_0^{PC} \approx 200 \mu\Omega\text{cm}$ (calculated using $d=80$ nm and Eq. (1), where a small contribution of the first term is neglected), what is 5 times larger than the bulk value! Accordingly, the elastic mean free path of electrons in PC will be 5 times smaller and amounts to only a few nanometers. All these estimations exclude the ballistic regime and promote the realization of the thermal regime of the current flow with a voltage rise. This point will be checked further by analyzing the measured $dV/dI(V)$ in the thermal regime.

IV. ANALYZING IN THE THERMAL REGIME

In the case of thermal regime, when the contact size d becomes much larger than the inelastic electron mean-free path, the temperature inside PC increases with the bias voltage according to the well-known relation^{3,5}:

$$T_{PC}^2 = T_{bath}^2 + V^2/4L_0, \quad (2)$$

where T_{PC} is the temperature in the PC core, T_{bath} is the temperature of the bath, and L_0 is the Lorentz number ($L_0 = 2.45 \cdot 10^{-8} \text{ V}^2/\text{K}^2$).

Using Kulik's thermal model^{5,9}, the $I(V)$ characteristics of the PC and its derivative can be calculated from the temperature dependence of the resistivity $\rho(T)$ of the material under study:

$$I(V) = Vd \int_0^1 \frac{dx}{\rho(T_{PC}\sqrt{(1-x^2)})}. \quad (3)$$

Applying this formula, we have calculated $dV/dI(V)$ in the thermal regime using for the temperature dependence of the resistivity $\rho_{PC}(T)$ in PC a curve similar to $R(T)$ as shows the inset of Fig.1 with the residual resistivity $\rho_0^{PC} \approx 200 \mu\Omega\text{cm}$ estimated above. The obtained result shown in Fig.2 demonstrates the good qualitative and quantitative correlation with experimental data. Here we should note that the calculations result in diameter twice as large as $d=80 \text{ nm}$ determined above from the temperature dependencies. The reason is that Eq.(3) is derived for homocontact. We suppose that factor 2 must be included in the right part of Eq.(3) in the case of symmetric geometrically heterocontact. Therefore $d=80 \text{ nm}$ derived above should be compared with $d/2=77 \text{ nm}$ from Fig.2. Thus, the considered $dV/dI(V)$ curves correspond to the thermal regime of the current flow. A detailed analysis of the calculation of $dV/dI(V)$ in the thermal regime using bulk $\rho(T)$ data and the evolution of $dV/dI(V)$ for several temperatures is given below in Appendix A.

One of the pronounced features of the $dV/dI(V)$ characteristics is their asymmetry. All measured $dV/dI(V)$ curves are highly asymmetric having larger $dV/dI(V)$ values for the positive bias. Fig.3 presents the antisymmetric part $R^a(V)$ of $dV/dI(V)$ for the PC from Fig.1. The calculated $R^a(V)$ demonstrates the pronounced maximum at about 70 mV which becomes suppressed and shifts to the lower voltages at increasing temperature. Qualitatively, the shape of $R^a(V)$ curves at low temperature corresponds well to the temperature dependence of the thermopower $S(T)$ measured for the isostructural compound $\text{Ba}_{0.7}\text{K}_{0.3}\text{Fe}_2\text{As}_2$ ¹⁰ (see left inset in Fig.3). Additionally, the sign of the asymmetry is opposite to that found in $\text{SmFeAsO}_{1-x}\text{F}_x$ PCs¹¹, where the thermopower is also large, but negative. Besides, the temperature dependence of the maximum position in $R^a(V)$ follows a quadratic law (see right inset in Fig.3) which

is in accord with Eq.(2). All this confirms that the investigated PCs are in the thermal regime of the current flow, at least at high biases in the region of the maximum. In the case of heterocontact, $R^a(V)$ resembles the thermoelectric power of the investigated sample¹². Also the maximum of the normalized $R^a(V)$ in Fig.3 is high (up to 30%), what also coincides with the exceptionally high S as seen from Fig.3 (left inset).

The Lorentz number L in the investigated PC estimated from the slope of the T_{bath}^2 vs V^2 plot (see right inset in Fig.3) was found to deviate from the standard value being equal to about $2.5L_0$ which is close to the value we used for the calculation in Fig.2. This is an additional prove that the characteristic features of $dV/dI(V)$ – maxima and asymmetry can be described by the thermal model. An enhanced L may be due to the additional contribution of phonons to the thermal conductivity of PC through electrically non-conductive oscillant surfaces.

We collected $dV/dI(V)$ curves of different shape for several PCs in the left panels of Fig.4. Nevertheless, in all cases, the corresponding $R^a(V)$ data (right panels) show similar behavior and exhibit a maximum between 70 and 90 mV. The similar shape of $R^a(V)$ for different types of PCs testifies that this phenomenon is robust and that the asymmetry is mainly determined by the properties of the less disturbed bulk material (see Appendix B) while the PC itself plays here the role of a “heater” or “hot spot”.

We suggest that the thermal regime is realized also for PCs of other iron-based superconductors, which have similar high resistivity and thermopower. Therefore, $dV/dI(V)$ data in this case provide information that comes from $\rho(T)$ modified in PC core. The authors of Ref.¹³ reported, that they succeed to get PCs on [122]-type compounds free from heating. Their claim is based on the deviation of the behavior of the measured $dV/dI(V) = R(V)$ from that of $\rho(T)$. Thus, they state (see paragraph before summary in¹³), that the evidence of the non-thermal regime is “no agreement of bulk resistivity with dV/dI ”. At the same time, according to Eq.(1), $R(T)$ must behave similar to $\rho(T)$ in any case independently on the current regime, what we also demonstrate here (compare $R(T)$ and $\rho(T)$ in the insets of Fig.1 and Fig.10). Therefore, the interpretation of the PC data in¹³ should be not taken too literally.

The spectroscopic regime in PC can be confirmed by the presence of bosonic features in d^2V/dI^2 spectrum. It is known that the d^2V/dI^2 spectrum reflects the PC electron-phonon interaction function $\alpha^2F(\omega)$ ¹⁻³. The d^2V/dI^2 curves presented in Fig.5 shows a clear maximum at about 20 mV and a more smeared one around 60 mV. The measurements of the phonon density of states in isostructural BaFe_2As_2 by inelastic electron scattering¹⁴ showed a peak at similar energies ($\approx 21.5 \text{ meV}$) besides the more pronounced maxima at 13, 27 and 35 meV. The latter maxima correspond well to the theoretical calculation of the phonon density of state

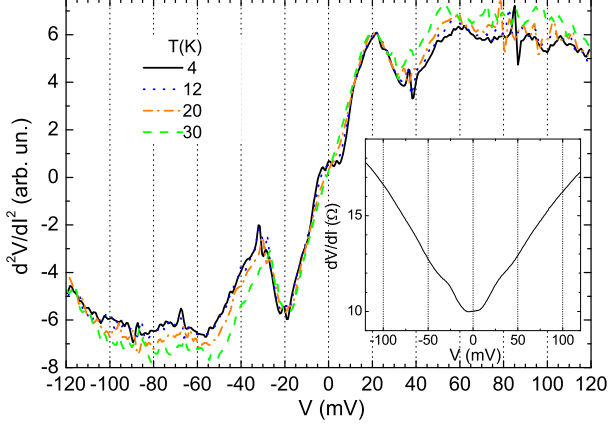


FIG. 5: (Color online) $d^2V/dI^2(V)$ of the $\text{Ba}_{0.75}\text{Na}_{0.25}\text{Fe}_2\text{As}_2\text{-Cu}$ PC with $R = 10\ \Omega$ measured at several temperatures. Inset: dV/dI of the same PC at $T=4\text{ K}$.

in BaFe_2As_2 . The authors claim, that the position of the peak at 21.5 meV is not predicted by the calculations, thus it may be due to electronic effects, e.g., Fermi-surface nesting. We should stress that mainly the backward scattering gives the largest contribution to the PC spectra of electron-phonon interaction³. But, as it was shown in Ref.¹⁵, the backward scattering is substantially suppressed in layered systems with strong electronic correlations. For the mentioned reason, the observation of the phonon modes in PC spectra of title compound can be complicated. Note, that the width of the peak at 20 mV remains almost unchanged at the temperature rise. At the same time, the phonon maxima should be smeared by the temperature increase, but this is not the case. Thus, the phonon nature of this peak is doubtful. However, we regularly measured such 20 mV maximum for KFe_2As_2 samples¹⁶ which indicates that this feature is not an artifact and should be intrinsic for [122]-type systems. Thus, additional investigations of that feature are needed.

V. PECULIARITIES IN THE SUPERCONDUCTING STATE

Let's turn to peculiarities of $dV/dI(V)$ appearing in the SC state, which are related to the Andreev-reflection spectroscopy of the SC gap. It concerns dV/dI minima at energies corresponding to the SC energy gap, which are shown in Fig. 6 for several PCs with different resistance. Such dV/dI characteristics correspond, presumably, the spectroscopic (diffusive) regime of the current flow at least at low biases. The dashed vertical stripes mark the position of the dV/dI minima which appear in the region between 6–9 meV for different PCs. Indeed, the

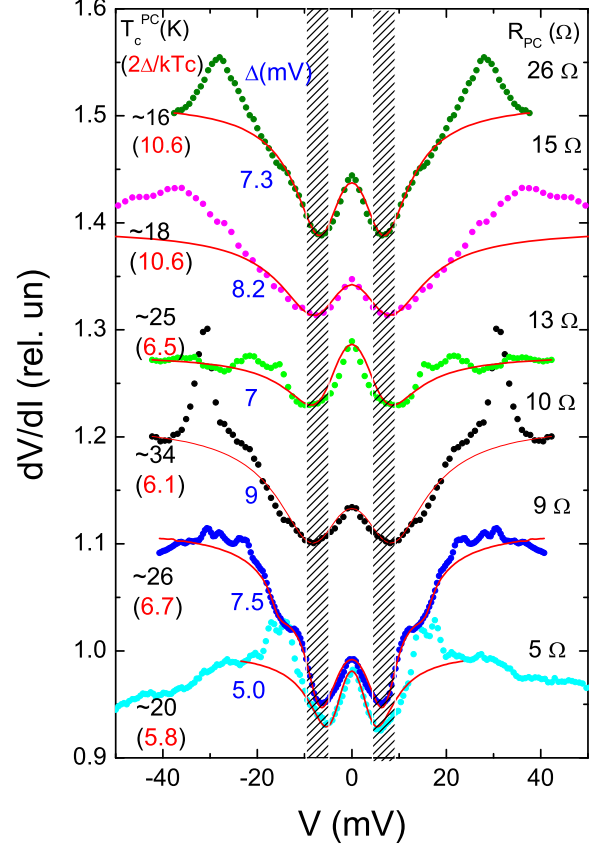


FIG. 6: (Color online) Normalized on the normal state $dV/dI(V)$ data (circles) displaying the AR-like features (minima around $V=0$) for the PCs with different resistance R_{PC} measured at 4 K. The dashed vertical stripes are placed to underline the position of the $dV/dI(V)$ minima which are related to the SC gap. T_c^{PC} is the approximate temperature at which SC features disappear in the presented $dV/dI(V)$. The BTK fit (dashed curves) is shown for each curve with values of Δ and $2\Delta/k_B T_c$. Two gap fit is shown Fig. 6 (see also Fig. 8). The curves are shifted for the sake of clarity.

gap value obtained from ARPES measurements⁶ for the compound with maximal T_c ($x=0.4$) is around 10.5 meV for the inner Γ barrel and around 3 meV for the outer Γ barrel, while for the underdoped sample with $x = 0.25$ the estimated gap is about 2 meV for the inner Γ barrel. So, the position of the minima in Fig. 6 corresponds more to the gap value for the compound with $x = 0.4$, albeit our samples have $x = 0.25$. It should be noted that the SC features in dV/dI presented in Fig. 6 disappeared at considerably higher temperature than the bulk $T_c \simeq 10\text{ K}$ for compound with $x=0.25$, likely due to a higher T_c of the surface because of its inhomogeneity. That is, PCs have a larger local T_c^{PC} than the bulk T_c .

We fitted $dV/dI(V)$ in Fig. 6 by widely accepted BTK model (see, e.g. Ref.⁴) to determine the gap value more

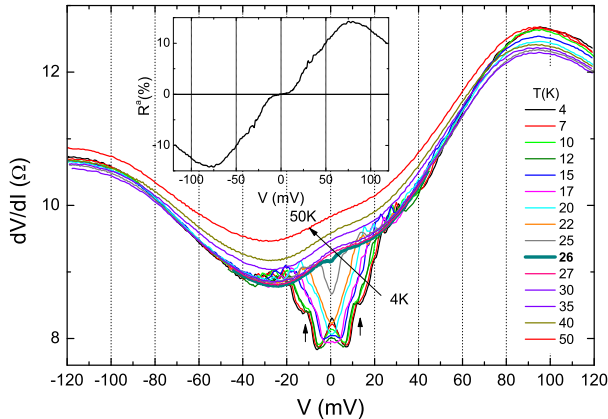


FIG. 7: (Color online) $dV/dI(V)$ of the PC with $R \approx 9 \Omega$ which exhibits additional minima seen at low temperatures (marked by the arrows). The thick curve at 26 K separates SC features (with minima) from normal state behavior. Thus, $T = 26$ K can be taken as a local T_c . Inset: reduced antisymmetric part R^a calculated for curve at $T = 4$ K.

precisely. As it is seen from Fig. 6, the gap value is distributed between 5 and 9 meV, that is it corresponds, in general, to the minima position in $dV/dI(V)$. At the same time the reduced gap $2\Delta/k_B T_c$ concentrated around 6 for 4 PCs from the bottom and around 10 for two upper PCs if we take into account local T_c^{PC} . This correlates with the values reported in¹⁷ for $\text{Ba}_{1-x}\text{K}_x\text{Fe}_2\text{As}_2$, namely, $2\Delta/k_B T_c = 2.5-4$ for a small and 9–10 for a large gap.

We have measured a few $dV/dI(V)$ characteristics where the second pair of minima can be connected, supposedly, to the second larger SC gap. The temperature series for such PC is shown in Fig. 7. We have fitted these $dV/dI(V)$ using the conventional two-gap approach⁴ and found a satisfactory agreement between the experimental and calculated curves with the SC gap values $\Delta_1 \approx 7.5$ meV and $\Delta_2 \approx 16$ meV at low temperatures (Fig. 8). Using the fit we have received the temperature dependence of both SC gaps along with the utilized fitting parameters, i.e. the barrier strength Z and broadening parameters Γ . However, the fit at higher temperatures becomes worse (especially by approaching the local T_c^{PC}), what can be seen also from the scattering of the fitting parameters in Fig. 8. Also, the contribution of the large gap to the fit amounts to about 10% only, similar as for a few other PCs with resembling AR features.

The estimated values of $2\Delta/k_B T_c$ for this PC are turned out to be quite high, about 8 and 18 for the small and the larger gap, respectively, when we take $T_c \approx 21$ K from the extrapolation of the gap dependence by the BCS curve (see Fig. 8). If we take the local $T_c \approx 26$ K from Fig. 7, then the reduced $2\Delta/k_B T_c$ value will be ≈ 7 for the small gap and still unrealistically large ≈ 15 for

the large gap. So, the features which we have taken as a larger gap are, apparently, of different origin, while the much more reproducible minima around ± 6 mV are caused by the SC gap likely for the inner Γ barrel. If the bias voltage further increases, $dV/dI(V)$ displays a broad maximum (Fig. 7) at about 90 mV and an asymmetric feature similar to that for PC in Fig. 1. Thus, the contact region passes into the thermal regime. An additional evidence for the nonspectroscopic origin of the second pair of minima is the behavior of $R^a(V)$ for this PC shown in the inset of Fig. 7. At the energies of these peculiarities, $R^a(V)$ starts deviate from zero what testifies that temperature in the PC core increases above T_c . This raises doubts that the mentioned features are due to the second SC gap.

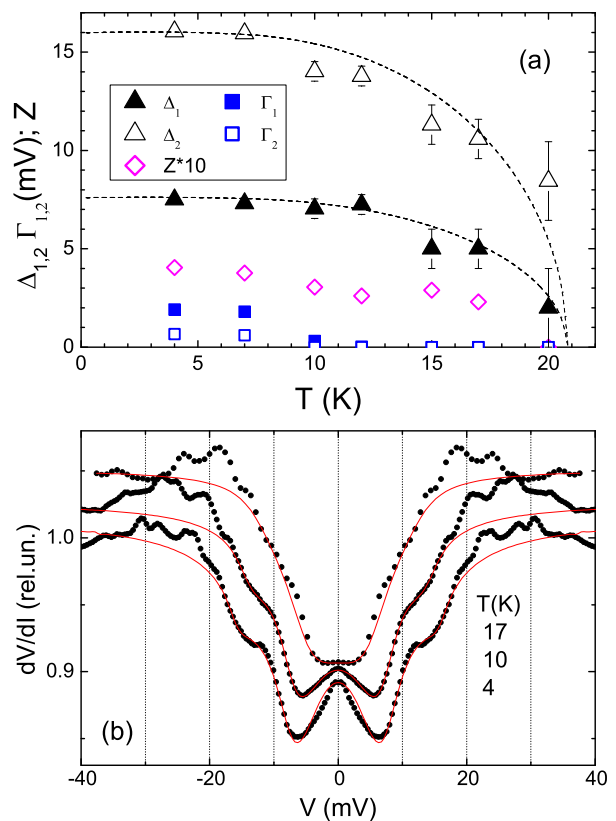


FIG. 8: (Color online) (a) Temperature dependence of the SC gaps Δ , broadening parameters Γ , barrier strengths Z received from the BTK fit in the two-gap approach for the PC from Fig. 7. The contribution of the smaller gap turned out to be in the range 80–90%. Dashed lines are BCS-like curves. (b) Examples of the experimental dV/dI (points) and calculated ones (lines) within the two-gap fit curves for several temperature values ($T = 4, 10$, and 17 K).

It is also necessary to take into account that the larger gap should be more suppressed and smeared by elastic scattering than the small one¹⁸. Furthermore, the re-

cent STM measurements on similar [122] compounds^{19,20} demonstrate that SC gap varies by factor two over scanned region of about 10 nm. The size of PC is at least a few times larger, as it was estimated above. That is, we measure by PC some averaged gap or, it is not excluded, merging of small and large gaps. Apparently, the more reproducible value of $2\Delta/k_B T_c$ of about 6, corresponds to such averaged gap. Interesting, that measured in²⁰ all dI/dV display only one pair of coherence maxima corresponding to a single gap. Further, much broader coherence maxima from the larger gap can be identified in¹⁹ only in some “bright” region. All this testify that the large gap is more difficult to uncover.

VI. CONCLUSIONS

Our PC study of iron-based superconductor $\text{Ba}_{1-x}\text{Na}_x\text{Fe}_2\text{As}_2$ ($x \approx 0.25$) shows that the current regime in PCs is at least diffusive at low biases and it crosses to the thermal regime for increasing bias. In this case, pronounced peculiarities in $dV/dI(V)$ data at high biases such as maxima and asymmetry are caused by the specific resistivity $\rho(T)$ and the thermopower $S(T)$ behavior versus temperature. The steep increase (or kink) in $\rho(T)$ due to the antiferromagnetic transition produces dV/dI maxima and thermoelectric effects result in the asymmetry of $dV/dI(V)$, which is well pronounced because of the large thermopower in this system. We suppose that the thermal regime (or heating) starts when antisymmetric part of $dV/dI(V)$ begins deviate from zero, what can be used to distinguish between thermal and not thermal current flow in PCs. We should also emphasize that an important selection rule for PC used for investigation of normal state and SC properties of materials is the similarity between $R_{PC}(T, V = 0)$ and the bulk $\rho(T)$. A discrepancy between them testifies that the substance in the PC core is disturbed and all information taken from such PC spectra must be interpreted with circumspection. Meanwhile, reproducible zero-bias minima detected in $dV/dI(V)$ data in the range $\pm(6-9)$ mV well below T_c could be connected with the manifestation of the SC gap. Features related to a second gap turned out hard to resolve unambiguously, likely due to enhanced elastic scattering, spatial inhomogeneity (reported in STM measurements) and transition to a thermal regime. It is not excluded also merging of small and large gaps because of interband scattering caused by impurities.

Acknowledgements

Yu.G.N. and O.E.K. thank V. Grinenko for assistance, the IFW Dresden for hospitality and the Alexander von Humboldt Foundation for financial support in the frame of a research group linkage program.

Appendix A

In this Appendix we demonstrate the effect of the residual resistivity, temperature and particular shape of $\rho(T)$ on the dV/dI curves calculated with Eq.(3). The calculated dV/dI curve in Fig. 2 shows a good correlation with the experimental data, when we used experimentally corrected resistivity for PC. Here we performed a more detailed calculation and analysis of PC $dV/dI(V)$ characteristics in the thermal regime using also the bulk resistivity $\rho(T)$ for $\text{Ba}_{0.75}\text{Na}_{0.25}\text{Fe}_2\text{As}_2$ taken from Ref.⁶. The calculations are shown in Fig. 9 for different values of residual resistivity ρ_0 at 4 K. Our experimental $dV/dI(V)$ in Fig. 2 have smaller amplitude and a broader maximum as compared to the theoretical calculations. This can be due to a higher residual resistance ρ_0 in the PC core caused by a non-perfect structure at the interface, surface impurities, stress induced defects by PC formation etc. As shown in Fig. 9, the specific value of the residual resistivity does not affect the position of the maximum of $dV/dI(V)$, however, the maximum becomes smaller for increasing ρ_0 . In the left inset, we show the $I(V)$ curve for the case of $\rho_0 = 0$. It has the specific N -like shape, where $dV/dI(V)$ diverges at the extrema of the $I(V)$ curve. We have not observed such $I(V)$ in this study, but we have measured the N -like shaped $I(V)$ for UPd_2Al_3 compound with similar behavior (steep increase) of $\rho(T)$ ²¹, what proves the calculations.

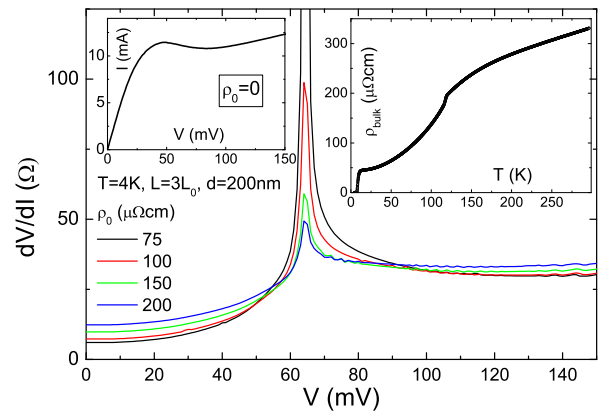


FIG. 9: (Color online) dV/dI curves calculated from Eqs. (2),(3) at 4 K for several values of residual resistivity using the bulk $\rho(T)$ of $\text{Ba}_{0.75}\text{Na}_{0.25}\text{Fe}_2\text{As}_2$ shown in the right inset. Left inset: calculated $I(V)$ curve for $\rho_0 = 0$.

We have calculated the $dV/dI(V)$ for $\rho_0 = 200 \mu\Omega\text{cm}$ (as estimated for the PC from Fig. 1) at different temperatures (Fig. 10). It turns out that the position of the $dV/dI(V)$ maximum shifts to lower energies as the temperature rises. Furthermore its position versus temperature follows a quadratic law (see inset in Fig. 10) in accord with Eq. (2) supporting our assumption of the thermal

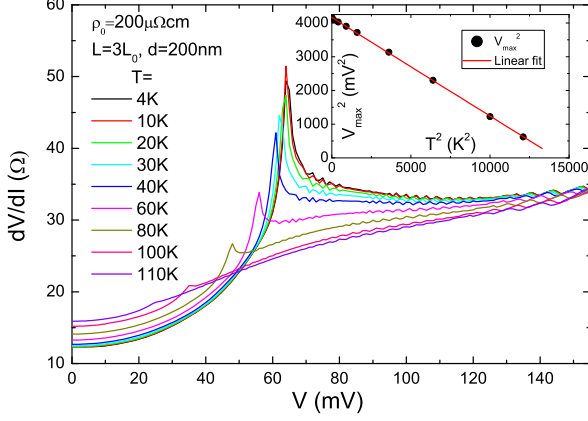


FIG. 10: (Color online) dV/dI curves calculated from Eqs. (2),(3) at several temperatures for $\rho_0 = 200 \mu\Omega\text{cm}$ using bulk $\rho(T)$ of $\text{Ba}_{0.75}\text{Na}_{0.25}\text{Fe}_2\text{As}_2$. Inset: position of maximum in dV/dI vs temperature in quadratic coordinates.

regime of the current flow through the PC.

It is naturally to suppose that not only the residual resistivity in the PC is enhanced as compared to the bulk, but also $\rho(T)$ in PC core might be modified. To model this situation, we slightly smoothed the $\rho(T)$ data between $\sim 100\text{K}$ and 150K as shown in the inset of Fig. 11. The smoothing of the sharp kink in $\rho(T)$ leads also to a smearing of the corresponding maximum in $dV/dI(V)$ (see Fig. 11). Here we again present the calculated $dV/dI(V)$ for different values of ρ_0 at $T=4\text{K}$ using the smoothed $\rho(T)$ dependence shown in the inset.

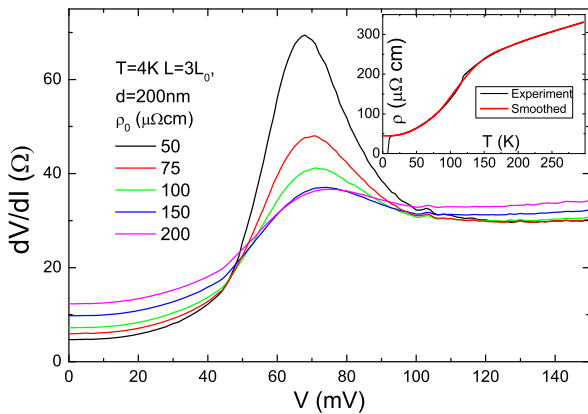


FIG. 11: (Color online) dV/dI curves calculated from Eqs. (2),(3) at 4K for several values of ρ_0 using the smoothed $\rho(T)$ dependence (thick red curve) of $\text{Ba}_{0.75}\text{Na}_{0.25}\text{Fe}_2\text{As}_2$ shown in the inset, where the thin black curve shows original $\rho(T)$.

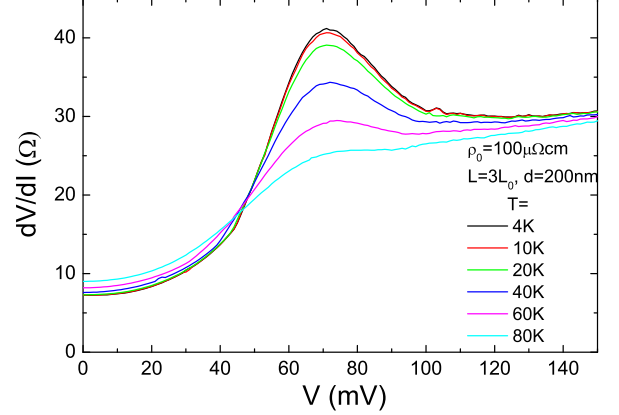


FIG. 12: (Color online) dV/dI curves calculated from Eqs. (2),(3) at several temperatures for $\rho_0 = 100 \mu\Omega\text{cm}$ using the smoothed $\rho(T)$ dependence from Fig. 11 (inset).

In Fig. 12, the calculated temperature variation of $dV/dI(V)$ for $\rho_0 = 100 \mu\Omega\text{cm}$ is presented. It is seen that the calculated $dV/dI(V)$ curves have a similar shape as the measured $dV/dI(V)$ data shown in Fig. 7. In this specific case, the maximum broadens and even slightly shifts to larger voltages for increasing temperature, whereas in Fig. 10 a shift of the sharp maximum to smaller voltages is observed for increasing temperature. Thus, it depends on the shape of the resistivity $\rho(T)$ in which direction the maximum of dV/dI is shifted as function of the temperature in the thermal regime of the current flow. Only, if the maximum in dV/dI is quite sharp, its position shifts according to Eq. (2).

Finally, due to enhanced local T_c observed for many PCs, we have also calculated $dV/dI(V)$ from $\rho(T)$ for a compound with $x = 0.35$ and $T_c = 30\text{K}$. Fig. 13 presents the calculated $dV/dI(V)$ for different ρ_0 based on $\rho(T)$ of this compound (see right inset in Fig. 13). The $I(V)$ characteristic for $\rho_0 = 0$ has again the N-shape, while for increasing ρ_0 a broadening and shifting of the dV/dI maximum to larger voltages is found. The temperature variation of $dV/dI(V)$ for $\rho_0 = 40 \mu\Omega\text{cm}$ plotted in Fig. 14 shows a broadening and shift of the $dV/dI(V)$ maximum to larger voltages for increasing temperature. The position of the maximum in $dV/dI(V)$ versus temperature follows approximately a quadratic law, but opposite to that in inset in Fig. 10.

Summarizing our calculations, we should note that:

- We can reproduce the measured $dV/dI(V)$ supposing the realization of the thermal regime in PCs and some modification of $\rho(T)$ in the contact core.
- The position of the peculiarities (peaks) of $dV/dI(V)$ characteristics in the thermal regime can be shifted both to lower voltages (for sharp peaks)

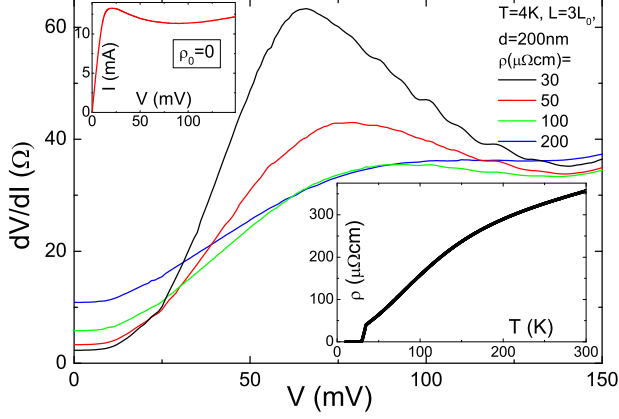


FIG. 13: (Color online) dV/dI curves calculated from Eqs. (2),(3) at 4K for several values of ρ_0 using $\rho(T)$ of $\text{Ba}_{0.65}\text{Na}_{0.35}\text{Fe}_2\text{As}_2$ ⁶ shown in the right inset. Left inset: calculated $I(V)$ curve for $\rho_0 = 0$.

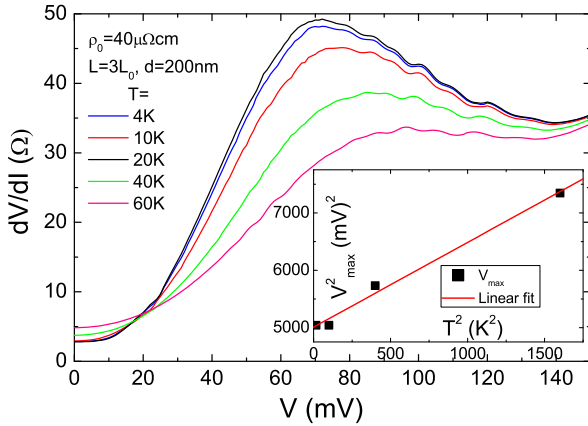


FIG. 14: (Color online) dV/dI curves calculated from Eqs. (2),(3) at several temperatures for $\rho_0 = 40 \mu\Omega\text{cm}$ using $\rho(T)$ of $\text{Ba}_{0.65}\text{Na}_{0.35}\text{Fe}_2\text{As}_2$. Inset: the position of maximum in dV/dI versus temperature in the quadratic coordinates.

as well as to higher voltages (for broad maxima) as the temperature rises.

- The variation of the peak position with temperatures can be described by Eq. (2) only if the peculiarities are quite sharp.

Appendix B

We should note that $dV/dI(V)$ remain asymmetric in the SC state below T_c (see, e.g., the data at 4.5K in

Fig. 1). However, it is known that the thermopower of any conductor equals to zero in the SC state. That is why the investigated superconductor in the contact region should be in the normal state at biases larger than the energy of SC peculiarities (gaps) of $dV/dI(V)$. It takes place because of heating and transition of the PC core in the normal state at a voltage increase. Next, as it was shown by Kulik²², in the thermal regime the temperature within the PC decreases gradually (from its maximum value in the plane of the PC) along the z -axis perpendicular to the plane (see Fig. 15). At the same time, as Fig. 15 shows, the potential drops much faster from the PC center than the temperature decreases. Thus, at a distance $\approx 2.5d$ from the PC center the potential deviates only on a few percents from its equilibrium, while the temperature at this distance still amounts a half from that in the PC center (see Fig. 15). Moreover, for heterocontacts in the thermal limit the maximal temperature is achieved in the metal with the larger resistivity and not in the PC center²³. Thus, due to heating, "hot spot" or the normal state region spreads effectively further from PC core (where main potential gradient is concentrated) and it has properties more close to the bulk material, what is reflected in a more reproducible shape of the antisymmetric part of the dV/dI of the PC in Fig. 4 with different raw dV/dI behavior.

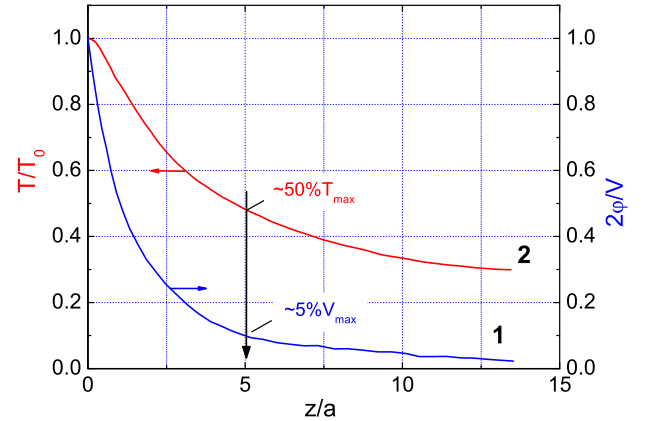


FIG. 15: (Color online) Distribution of the potential (1) and temperature (2) from the PC center $z=0$ along the z -axis perpendicular to the plane of PC in the thermal regime after Kulik theory²². Long vertical arrow marks the residual potential and temperature values at $z = 5a$, where $a = d/2$ is the PC radius.

- ¹ I.K.Yanson, Zh. Eksp. Teor. Fiz. **66**, 1035 (1974) [Sov. Phys. JETP **39**, 506 (1974)].
- ² A.V. Khotkevich, I.K. Yanson, Atlas of Point-Contact Spectra of Electron-Phonon Interaction in Metals (Kluwer Academic Publishers, Boston) 1995.
- ³ Yu. G. Naidyuk and I. K. Yanson, Point-Contact Spectroscopy, Springer Series in Solid-State Sciences (Springer Science+Business Media, Inc), vol. 145, 2005.
- ⁴ D. Daghero, M.Tortello, G.A. Ummarino and R.S. Gonnelli, Rep. Prog. Phys. **74**, 124509 (2011).
- ⁵ B. I. Verkin, I. K. Yanson, I. O. Kulik, O.I. Shklyarevski, A.A. Lysykh, Yu. G. Naidyuk, Solid State Commun. **30**, 215 (1979).
- ⁶ S. Aswartham, M. Abdel-Hafiez, D.Bombor, M.Kumar, A.U.B. Wolter, C.Hess, D.V.Evtushinsky, V. B. Zabolotnyy, A. A. Kordyuk, T. K. Kim, S. V. Borisenko, G. Behr, B. Büchner, and S. Wurmehl, Phys.Rev. B **85**, 224520 (2012).
- ⁷ Bing Shen, Huan Yang, Zhao-Sheng Wang, Fei Han, Bin Zeng, Lei Shan, Cong Ren, and Hai-Hu Wen, Phys. Rev. B **84**, 184512 (2011).
- ⁸ L. Wray, D. Qian, D. Hsieh, Y. Xia, L. Li, J. G. Checkelsky, A. Pasupathy, K. K. Gomes, C. V. Parker, A. V. Fedorov, G. F. Chen, J. L. Luo, A. Yazdani, N. P. Ong, N. L. Wang, and M. Z. Hasan, Phys. Rev. B **78**, 184508 (2008).
- ⁹ I. O. Kulik, Fiz. Nizk. Temp. **18**, 440 (1992) [Sov. J. Low Temp. Phys. **18**, 302 (1992)].
- ¹⁰ Y. J. Yan, X. F. Wang, R. H. Liu, H. Chen, Y. L. Xie, J. J. Ying, and X. H. Chen, Phys. Rev. B **81**, 235107 (2010).
- ¹¹ Yu. G. Naidyuk, O. E. Kvitnitskaya, I. K. Yanson, G. Fuchs, S. Haindl, M. Kidszun, L. Schultz and B. Holzapfel, Supercond. Sci. Technol. **24**, 065010 (2011).
- ¹² Yu. G. Naidyuk, N. N. Gribov, A. A. Lysykh, I. K. Yanson, N. B. Brandt, V. V. Moshchalkov, Pis'ma Zh. Exp. Teor. Phys. **41**, 325 (1985) [JETP Lett. **41**, 399 (1985)].
- ¹³ H. Z. Arham, C. R. Hunt, W. K. Park, J. Gillett, S. D. Das, S. E. Sebastian, Z. J. Xu, J. S. Wen, Z. W. Lin, Q. Li, G. Gu, A. Thaler, S. Ran, S. L. Bud'ko, P. C. Canfield, D. Y. Chung, M. G. Kanatzidis, and L. H. Greene, Phys. Rev. B **85**, 214515 (2012).
- ¹⁴ R. Mittal, Y. Su, S. Rols, T. Chatterji, S. L. Chaplot, H. Schober, M. Rotter, D. Johrendt, and Th. Brueckel, Phys. Rev. B **78**, 104514 (2008).
- ¹⁵ M. L. Kubic, Physics Reports **338**, 1 (2000).
- ¹⁶ Yu. G. Naidyuk, O. E. Kvitnitskaya, N. V. Gamayunova, S. Aswartham, S. Wurmehl, D.V. Efremov, G. Fuchs, S.-L. Drechsler, Thesis of Trilateral Russia-Ukraine-Germany workshop on Hot Topics in HTSC: Fe-Based Superconductors, Zvenigorod (Moscow district) Sept. 29–Oct. 2, (2013) (to be published).
- ¹⁷ P. Szabó, Z. Pribulová, G. Pristáš, S. L. Bud'ko, P. C. Canfield, and P. Samuely, Phys. Rev. B **79**, 012503 (2009).
- ¹⁸ D. V. Efremov, M. M. Korshunov, O. V. Dolgov, A. A. Golubov, and P. J. Hirschfeld, Phys. Rev. B **84**, 180512(R) (2011); D. V. Efremov, A. A. Golubov and O. V. Dolgov, New Journal of Physics **15**, 013002 (2013).
- ¹⁹ Lei Shan, Yong-Lei Wang, Bing Shen, Bin Zeng, Yan Huang, Ang Li, DaWang, Huan Yang, Cong Ren, Qiang-Hua Wang, Shuheng H. Pan and Hai-Hu Wen, Nature Phys. **4**, 325 (2011).
- ²⁰ Can-Li Song, Yi Yin, Martin Zech, Tess Williams, Michael M. Yee, Gen-Fu Chen, Jian-Lin Luo, Nan-Lin Wang, E. W. Hudson, and Jennifer E. Hoffman, Phys. Rev. B **87**, 214519 (2013).
- ²¹ Yu. G. Naidyuk, K. Gloos, I. K. Yanson and N. K. Sato, J. Phys.: Condens. Matter **16**, 3433 (2004).
- ²² I. O. Kulik, Thermal spectroscopy of phonons in normal metal point contacts, Preprint No. 8-84, Kharkov (1984) (in Russian).
- ²³ I. F. Itskovich, I. O. Kulik and R. I. Shekhter, Fiz. Nizk. Temp. **11**, 886 (1992) [Sov. J. Low Temp. Phys. **11**, 649 (1985)].